

Mini-discs around spinning black holes

I. Zalamea^{*} and A. M. Beloborodov[†]

Physics Department and Columbia Astrophysics Laboratory, Columbia University, New York, NY 10027, USA

Accepted —. Received —; in original form —

ABSTRACT

Accretion onto black holes in wind-fed binaries and in collapsars forms small rotating discs with peculiar properties. Such “mini-discs” accrete on the free-fall time without help of viscosity and nevertheless can have a high radiative efficiency. The inviscid mini-disc model was previously constructed for a non-rotating black hole. We extend the model to the case of a spinning black hole, calculate the structure and radiative efficiency of the disc and find their dependence on the black hole spin. If the angular momenta of the disc and the black hole are anti-aligned, a hydrodynamic analog of Penrose process takes place.

Key words: accretion, accretion discs — black hole physics.

1 INTRODUCTION

The mini-disc model was motivated by the estimate for angular momentum of accretion flows, l , in wind-fed X-ray binaries (Illarionov & Sunyaev 1975; Shapiro & Lightman 1976; Illarionov & Beloborodov 2001). These systems happen to have $l \sim r_g c$, where $r_g = 2GM/c^2$ is the gravitational radius of the black hole. It is marginally sufficient to form a centrifugally supported disc. Then a small disc can form, which is not supported centrifugally and instead accretes on the free-fall time (Beloborodov & Illarionov 2001, hereafter BI01). The mini-disc accretes so fast (super-sonically) that the effects of viscosity can be neglected. A similar disc may form inside collapsing stars (Lee & Ramirez-Ruiz 2006; Beloborodov 2008).

The mini-disc can be thought of as a caustic in the equatorial plane of a rotating accretion flow. It absorbs the feeding infall, and this interaction releases energy, making the accretion radiatively efficient. With increasing angular momentum, the size of the disc grows up to $14r_g c$, and at this point the centrifugal barrier stops accretion, so that it can proceed only on a viscous timescale. Thus, the mini-disc model fills the gap between two classical regimes of accretion — spherical ($l < r_g c$, Bondi 1952) and standard accretion disc ($l \gg r_g c$, Shakura & Sunyaev 1973) — and is qualitatively different from both.

The calculations of BI01 were limited to the case of a Schwarzschild black hole. In the present paper we study the mini-disc around Kerr black holes. The model is constructed under the following assumptions:

- (i) The flow is axially symmetric. We assume that the rotational axes of the accretion flow and the black hole are aligned (or anti-aligned).
- (ii) The flow is symmetric under reflection about the equatorial plane. The symmetric streamlines collide in the equatorial plane and form a ring-like caustic around the black hole.
- (iii) The flow falls freely (ballistically) from a large radius $r \gg r_g$ until it hits the caustic; its pressure is negligible everywhere except in the mini-disc. This assumption is valid if the flow is cooled efficiently (by radiation in X-ray binaries or by neutrinos in collapsars). The heat released in the shocks that accompany the disc-infall interaction is assumed to be quickly radiated away, so that the shocks stay near the disc plane, forming a “sandwich”. The validity of this assumption is discussed in BI01 for the case of X-ray binaries and in Beloborodov (2008) for collapsars.
- (iv) The flow is quasi-steady: its accretion rate and angular momentum remain constant on the timescale of accretion through the mini-disc (which is comparable to the free-fall time from $r \sim 10r_g$).

The paper is organized as follows. Section 2 describes the parabolic ballistic infall in Kerr metric and its ring caustic in the equatorial plane. In section 3 we write down the equations that govern the gas motion in the caustic (the mini-disc) and solve the equations numerically. In section 4 we calculate the total luminosity of the disc observed at infinity, taking into account the light capture into the black hole.

^{*} E-mail: izalamea@phys.columbia.edu

[†] Also at Astro-Space Center of Lebedev Physical Institute, Profsojuznaja 84/32, Moscow 117810, Russia

2 SUPERSONIC INFALL WITH ANGULAR MOMENTUM

The spacetime of a black hole of mass M and angular momentum J is described by the Kerr metric. In Boyer-Lindquist coordinates (ct, r, θ, ϕ) the metric is given by

$$g_{ij}dx^i dx^j = - \left(1 - \frac{r_g r}{\rho^2}\right) (cdt)^2 - \frac{2r_g ar}{\rho^2} \sin^2 \theta (cdt) d\phi + \frac{\rho^2}{\Delta} dr^2 + \rho^2 d\theta^2 + \frac{\sin^2 \theta}{\rho^2} + [(r^2 + a^2)^2 - a^2 \Delta \sin^2 \theta] d\phi^2, \quad (1)$$

$$\rho^2 = r^2 + a^2 \cos^2 \theta, \quad (2)$$

$$\Delta = r^2 - r_g r + a^2. \quad (3)$$

The spin parameter of the black hole $a = J/Mc$ has dimension of cm and must be in the interval $|a| \leq r_g/2 = GM/c^2$. Throughout the paper we shall also use the dimensionless parameter $a_* = ac^2/GM$, $|a_*| \leq 1$.

We assume that the gas infall forms at a large radius $r \gg r_g$, where it is efficiently cooled and, like dust, begins to fall freely towards the black hole. A streamline of this ballistic infall is determined by three integrals of motion: specific angular momentum l , its projection l_z on the spin axis of the black hole, and specific orbital energy $E \approx c^2$ (the infall is nearly parabolic). The four-velocity of a parabolic free-fall in Kerr metric is given by (e.g. Misner et al. 1973),

$$\rho^2 \frac{dr}{d\tau} = \pm c\sqrt{R}, \quad (4)$$

$$\rho^2 \frac{d\theta}{d\tau} = \pm \sqrt{\Theta}, \quad (5)$$

$$\rho^2 \frac{d\phi}{d\tau} = \frac{1}{\Delta} (cr_g ar - a^2 l_z) + \frac{l_z}{\sin^2 \theta}, \quad (6)$$

$$\rho^2 \frac{dt}{d\tau} = \frac{1}{\Delta} \left[(r^2 + a^2)^2 - r_g ar \frac{l_z}{c} \right] - a^2 \sin^2 \theta, \quad (7)$$

where $l_z = l \sin \theta_\infty$, θ_∞ is the asymptotic polar angle of a streamline at large r , and

$$R(r) = r_g r^3 - \frac{l^2}{c^2} r^2 \left(1 - \frac{r_g}{r}\right) - 2r_g a \frac{l}{c} r \sin \theta_\infty + a^2 \left(r_g r - \frac{l^2}{c^2} \cos^2 \theta_\infty \right), \quad (8)$$

$$\Theta(\theta) = l_z^2 (\cot^2 \theta_\infty - \cot^2 \theta). \quad (9)$$

The ballistic accretion flow is completely specified by the distribution of its density and angular momentum on a sphere of a large radius $r \gg r_g$. As the gas approaches the black hole and develops a significant rotational velocity, the infall is deflected from pure radial motion, and its streamlines intersect in the equatorial plane. The radius of this collision is determined by the angular momentum of the colliding symmetric streamlines.

2.1 Collision Radius

The streamline coming from an asymptotic direction $(\theta_\infty, \phi_\infty)$ with angular momentum $l(\theta_\infty, \phi_\infty)$ reaches the equatorial plane and collides with the symmetric streamline at the radius r_* defined by

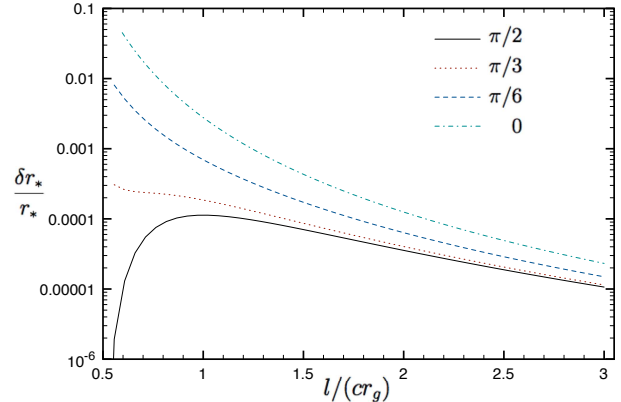


Figure 1. Fractional difference between the exact r_* and its approximation (eq. 11) as a function of l . The curves start at $l_0 = l_*$ that corresponds to r_* at the horizon of the black hole. All curves are plotted for maximally rotating black holes ($a_* = 1$), when eq. (11) is least accurate.

$$- \int_\infty^{r_*} \frac{dr}{\sqrt{R}} = \int_{\theta_\infty}^{\pi/2} \frac{cd\theta}{\sqrt{\Theta}} = \frac{\pi c}{2l}. \quad (10)$$

We solved this equation for r_* numerically (it involves an elliptic integral on the left-hand side). A good analytical approximation to r_* is given by

$$r_* \approx \frac{l^2}{GM} - r_g \left[\frac{10 - 3\pi}{4} \left(\frac{l_{eff}}{l} \right)^2 - \frac{48 - 15\pi}{16} \left(\frac{ac \cos \theta_\infty}{l} \right)^2 \right], \quad (11)$$

where $l_{eff}^2 \equiv l^2 + (ac)^2 - 2acl \sin \theta_\infty$. The accuracy of this approximation is shown in Figure 1. It is better than 3 per cent when r_* is outside the horizon, for any set of parameters relevant for the mini-disc formation.

The collision radius is maximum for the streamlines near the equatorial plane ($\theta_\infty \rightarrow \pi/2$). This defines the outer radius of the disc,

$$r_d = r_* \left(\theta_\infty = \frac{\pi}{2} \right). \quad (12)$$

2.2 Non-intersection of streamlines above the equatorial plane

The ballistic flow defines a mapping from the sphere $(\theta_\infty, \phi_\infty)$ to a sphere of radius r (cf. BI01): $(\theta_\infty, \phi_\infty) \rightarrow (\theta(r), \phi(r))$. The streamlines of the flow do not intersect before reaching the equatorial plane if the Jacobian of this mapping remains positive for all $r > r_*$, i.e.

$$\mathcal{J} = \text{Det} \begin{pmatrix} \frac{\partial \theta(r)}{\partial \theta_\infty} & \frac{\partial \phi(r)}{\partial \theta_\infty} \\ \frac{\partial \theta(r)}{\partial \phi_\infty} & \frac{\partial \phi(r)}{\partial \phi_\infty} \end{pmatrix} > 0. \quad (13)$$

This condition is equivalent to $\partial \theta(r)/\partial \theta_\infty > 0$. Using the relation between θ and r ,

$$\frac{\cos \theta(r)}{\cos \theta_\infty} = \cos \psi, \quad \psi \equiv \frac{l}{c} \int_r^\infty \frac{dr}{\sqrt{R}}, \quad (14)$$

one finds that $\mathcal{J} > 0$ if

$$\frac{d \cos \theta(r)}{d \cos \theta_\infty} = \cos \psi - \cos \theta_\infty \sin \psi \frac{d\psi}{d \cos \theta_\infty} > 0. \quad (15)$$

This condition must be checked for a given distribution of angular momentum $l(\theta_\infty)$. In the numerical examples below we assume a distribution of the form

$$l(\theta_\infty) = l_0 \sin \theta_\infty, \quad (16)$$

(rigid-body rotation at infinity). We find that the streamlines do not intersect before reaching the ring caustic in the equatorial plane.

3 DISC DYNAMICS

We consider here only accretion flows that are asymptotically spherical at $r \gg r_g$, i.e. we assume that the accretion rate at infinity is spherically symmetric, $d\dot{M}/d\Omega_\infty = \text{const} = \dot{M}_{\text{tot}}/4\pi$. Streamlines that start at θ_∞ with angular momentum $l(\theta_\infty)$ reach the equatorial caustic at a radius $r_*(\theta_\infty)$. The accretion rate through the disc at a radius r , $\dot{M}(r)$, equals the net accretion rate along the streamlines that enter the caustic outside r ,

$$\dot{M}(r) = \dot{M}_{\text{tot}} \cos \theta_\infty(r), \quad (17)$$

where $\theta_\infty(r)$ is the asymptotic polar angle of streamlines that collide at radius r . We find it by inverting the function $r_*(\theta_\infty)$.

Matter inside the disc moves horizontally with four-velocity $u^i = (u^t, u^r, 0, u^\phi)$ and density ρ . The disc is steady and axially symmetric, so u^i and ρ depend on r only. Equations for $u^i(r)$ and $\rho(r)$ are derived using the conservation laws for baryon number, energy and momentum. These laws are expressed by the following general equations (e.g. Landau & Lifshitz 1980),

$$\frac{1}{\sqrt{-g}} \partial_i (\sqrt{-g} \rho u^i) = 0, \quad (18)$$

$$\frac{1}{\sqrt{-g}} \partial_k (\sqrt{-g} T_i^k) = \frac{1}{2} \frac{\partial g_{kl}}{\partial x^i} T^{kl}, \quad (19)$$

where $T^{kl} = \rho c^2 u^k u^l$ is the stress-energy tensor; we assume that it is dust-like everywhere, i.e. neglect the internal energy density, pressure, and magnetic fields compared with ρc^2 . Above the disc, the stress-energy tensor is that of the ballistic infall. The infall four-velocity and density just above the disc shall be denoted by \hat{u}^i and $\hat{\rho}$, to distinguish them from the similar quantities inside the disc, u^i and ρ . Then the conservation laws (eqs. 18 and 19) give,

$$\frac{d\dot{M}}{dr} = -4\pi r^2 \hat{\rho} \hat{u}^\theta, \quad (20)$$

$$\frac{d}{dr} \left(\frac{h}{r} T_i^r \sqrt{-g} \right) + 2\sqrt{-g} \hat{T}_i^\theta = \frac{1}{2} \frac{h}{r} \sqrt{-g} \frac{\partial g_{kl}}{\partial x^i} T^{kl}. \quad (21)$$

Here $\dot{M} = 2\pi r h \rho u^r$, h is the thickness of the disc, and $\hat{T}^{kl} = \hat{\rho} c^2 \hat{u}^k \hat{u}^l$ is the stress-energy tensor of the infall. Using equation (20) one finds from equation (21)

$$\frac{d}{dr} (\dot{M} u_i) - \hat{u}_i \frac{d\dot{M}}{dr} = \frac{1}{2} \frac{\partial g_{kl}}{\partial x^i} u^k u^l \frac{\dot{M}}{u^r}. \quad (22)$$

For $i = \{t, \phi\}$ (conservation of energy and angular momentum) the right-hand side of this equation vanishes. In particular, for $i = \phi$ this equation gives

$$\frac{d(\dot{M} u_\phi)}{dr} = \hat{u}_\phi \frac{d\dot{M}}{dr}, \quad (23)$$

$$u_\phi(r) = -\frac{1}{\dot{M}(r)} \int_r^{r_d} \hat{u}_\phi \frac{d\dot{M}}{dr} dr. \quad (24)$$

For $l(\theta_\infty)$ given by equation (16) we have $\hat{u}_\phi \equiv l_z = l^2/l_0$ and, using equation (17), we find

$$u_\phi(r) = \frac{2}{3} l_0 + \frac{l^2(r)}{3l_0}. \quad (25)$$

For $i = r$, equation (22) expresses conservation of radial momentum. Its right-hand side does not vanish, and one needs to evaluate $\frac{\partial g_{kl}}{\partial r} u^k u^l$. Substituting $u^\phi = (u_\phi - g_{t\phi} u^t)/g_{\phi\phi}$, using $u_i u^i = -c^2$ and collecting terms one can write

$$\frac{\partial g_{kl}}{\partial r} u^k u^l = A + B(u^r)^2 + C u_\phi^2 + D u_\phi u^t, \quad (26)$$

where A, B, C and D are functions of r only,

$$A = -\frac{r_g c^2 [r^4 + a^4 + 2a^2 r(r - r_g)]}{r [a^2 + r(r - r_g)] [r^3 + a^2(r + r_g)]},$$

$$B = 2\partial_r g_{rr} - \frac{a^2 r (2r - 3r_g)}{[a^2 + r(r - r_g)] [r^3 + a^2(r + r_g)]},$$

$$C = \frac{r^4 (2r - 3r_g) - 2a^4 r_g + a^2 r (2r^2 - 3r_g r + 3r_g^2)}{[a^2 + r(r - r_g)] [r^3 + a^2(r + r_g)]^2},$$

$$D = -\frac{2ar_g (3r^2 + a^2)}{[r^3 + a^2(r + r_g)]^2}. \quad (27)$$

Equation (22) for $i = r$ becomes

$$\frac{du^r}{dr} = \frac{\hat{u}^r - u^r}{\dot{M}} \frac{d\dot{M}}{dr} + \frac{A + (B - 2\partial_r g_{rr})(u^r)^2 + C u_\phi^2 + D u_\phi u^t}{2g_{rr} u^r}. \quad (28)$$

Finally, u^t can be expressed in terms of u^r and u_ϕ from $u_i u^i = -c^2$,

$$(u^t)^2 = 1 + \frac{r_g (r^2 + a^2)}{r [a^2 + r(r - r_g)]} + \frac{u_\phi^2 / c^2}{a^2 + r(r - r_g)} + \frac{r^4 + a^2 r(r + r_g)}{[a^2 + r(r - r_g)]^2} \left(\frac{u^r}{c} \right)^2. \quad (29)$$

In equation (28) all quantities are known functions of radius except u^r . We solve numerically this differential equation for $u^r(r)$. Example solutions are shown in Fig. 2, where we plot the radial and azimuthal velocities measured by ZAMO (zero-angular-momentum observer at fixed r ; Appendix A gives the transformation of 4-vectors to the ZAMO frame).

If the angular-momentum parameter of the flow, l_0 , exceeds a critical value l_{cr} , accretion in the disc is stopped by the centrifugal barrier (u^r changes sign). For flows with $l_0 < l_{\text{cr}}$ the radial velocity remains everywhere negative. As l_0 approaches l_{cr} the trajectory of disc accretion makes more turns around the black hole (see Fig. 3) and at $l_0 = l_{\text{cr}}$ it

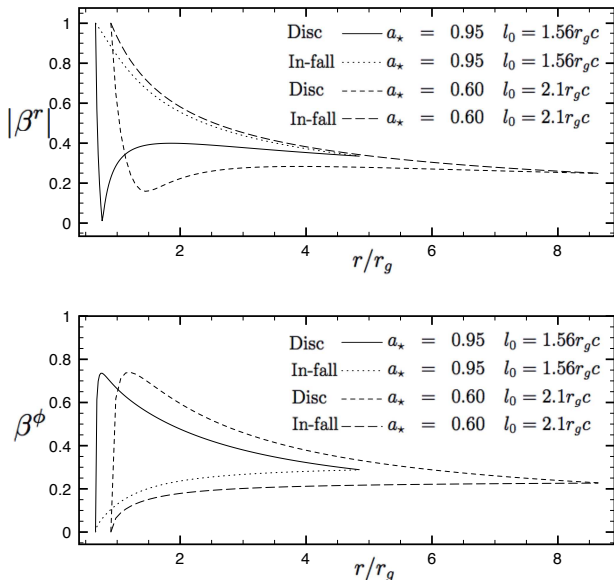


Figure 2. *Upper panel:* solutions for the radial velocity measured by ZAMO (in units of c) of the parabolic infall above the disc and the matter inside the disc. Two cases are shown: $a_* = 0.6$, $l_0 = 2.1r_g c$ and $a_* = 0.95$, $l_0 = 1.56r_g c$. *Lower panel:* the corresponding azimuthal velocities of the infall and the disc, measured by ZAMO.

makes infinite number of turns. Similar behavior was found for mini-discs around Schwarzschild black holes; in this case $l_{\text{cr}} = 2.62r_g c$ (BI01). For spinning black holes, l_{cr} depends on a_* . We have evaluated numerically $l_{\text{cr}}(a_*)$ and the corresponding maximum size of the mini-disc $r_d(a_*)$. The results are shown in Figure 4.

Figure 4 also shows the minimum value of l_0 , denoted by l_* , that is required to form a disc outside the black-hole horizon,

$$r_h(a_*) = \frac{1 + \sqrt{1 - a_*^2}}{2} r_g. \quad (30)$$

Accretion proceeds in the inviscid mini-disc regime when $l_* < l_0 < l_{\text{cr}}$. This range shrinks with increasing $a_* > 0$, and expands if $a_* < 0$ (which means that the black hole and the accretion flow rotate in the opposite directions).

Matter in the polar region of a quasi-spherical accretion flow falls directly into the black hole before crossing the equatorial plane. The mini-disc is formed in the other, equatorial part of the flow (cf. Fig. 1 in BI01). The boundary between these two accretion zones is determined by the condition $r_*(l) = r_h$. Equation (17) gives the fraction of \dot{M}_{tot} that accretes through the disc,

$$\frac{\dot{M}(r_h)}{\dot{M}_{\text{tot}}} = \cos \theta_\infty(r_h), \quad (31)$$

which depends on l_0 and a ; it is maximum when $l_0 = l_{\text{cr}}$. The maximum fraction is shown in Figure 5.

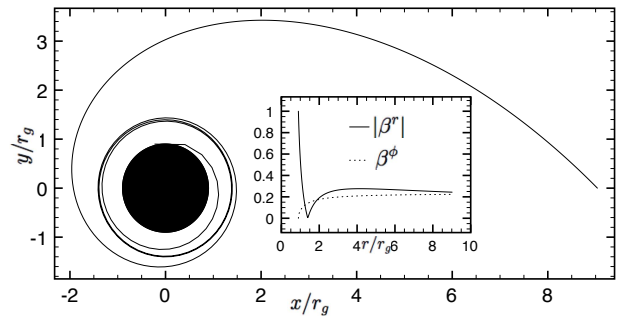


Figure 3. Trajectory of disc matter in the critical case $l_0 = 2.14r_g c$ for a black hole with $a_* = 0.6$. The insert shows the radial and azimuthal velocities of the disc measured by ZAMO. x and y are the coordinates in the equatorial plane defined by $x = r \cos \phi$, $y = r \sin \phi$.

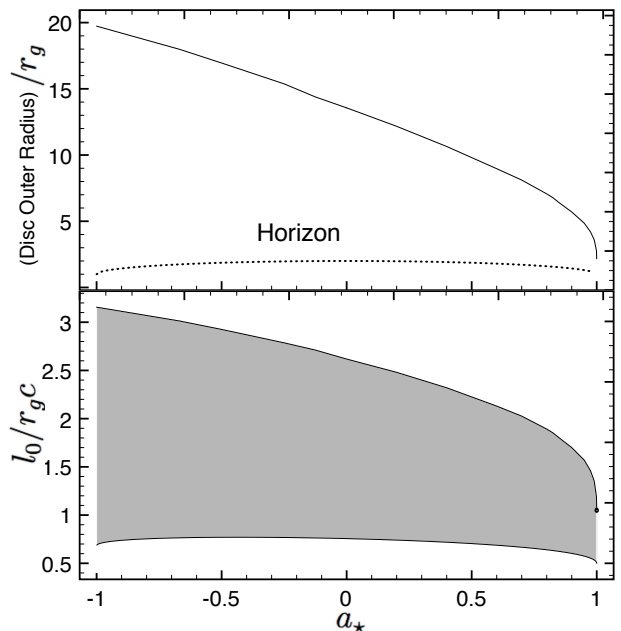


Figure 4. *Bottom panel:* the range of angular momenta $l_*(a_*) < l_0 < l_{\text{cr}}(a_*)$ that lead to the inviscid mini-disc regime (shaded region). Accretion with $l_0 < l_*$ is quasi-spherical all the way into the black hole; it does not form a caustic outside the horizon. Accretion with $l_0 > l_{\text{cr}}$ must proceed through a viscous, centrifugally supported disc. *Top panel:* maximum radius of the mini-disc ($l_0 = l_{\text{cr}}$) as a function of the black-hole spin parameter a_* (solid curve). The radius of the black hole $r_h(a_*)$ (eq. 30) is shown by the dotted curve.

4 DISC LUMINOSITY

The mini-disc is a radiative caustic that converts kinetic energy of the accretion flow to radiation. Let $L(r)$ be the total luminosity produced by the disc outside radius r . The law of energy conservation gives an explicit expression for the luminosity,

$$L(r) = [c^2 + cu_t(r)] \dot{M}(r), \quad (32)$$

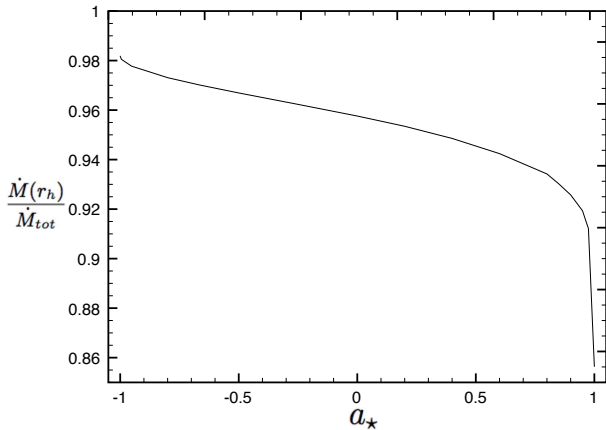


Figure 5. Maximum mass fraction accreted through the inviscid mini-disc. This maximum corresponds to $l_0 = l_{cr}$ and depends on the black-hole spin a_* (see the text).

where c^2 is the initial orbital energy of the accretion flow at infinity and $-cu_t(r)$ is the orbital energy of the disc material at radius r . It is found using the solution for $u^i(r)$ from section 3. The radial distribution of luminosity is given by dL/dr , and the total produced luminosity is $L = L(r_h)$. This luminosity would be received at infinity if no radiation were captured by the black hole.

When the capture effect is taken into account, the luminosity escaping to infinity may be written as

$$L_{\text{esc}} = \int_{r_h}^{r_d} \frac{dL}{dr} f_{\text{esc}}(r) dr, \quad (33)$$

where $f_{\text{esc}}(r)$ is the escaping fraction of radiation emitted at radius r ; the fraction $1 - f_{\text{esc}}$ is absorbed by the black hole. Assuming that the emission is approximately isotropic in the rest frame of the disc, we derive in Appendix A

$$f_{\text{esc}} = \left(1 - \frac{g_{t\phi}}{\sqrt{-\tilde{g}_{tt}g_{\phi\phi}}} \frac{\beta^\phi}{\gamma} \right)^{-1} \int_{S_{\text{esc}}} \frac{1 - \frac{g_{t\phi}\bar{\Omega}^\phi}{\sqrt{-\tilde{g}_{tt}g_{\phi\phi}}}}{\gamma^4(1 - \beta \cdot \bar{\Omega})^3} \frac{d\bar{\Omega}}{4\pi}, \quad (34)$$

where β is the disc velocity (in units of c) measured by ZAMO (zero-angular-momentum observer at fixed r), $\gamma = (1 - \beta^2)^{-1/2}$ and $\tilde{g}_{tt} = g_{tt} - g_{t\phi}^2/g_{\phi\phi}$. The integral is taken over the escape cone $S_{\text{esc}}(r)$ — all photon directions $\bar{\Omega}$ (in the ZAMO frame) that lead to escape. The calculation of these cones is described in Appendix A.

The resulting $L_{\text{esc}}(r)$ is found numerically. Figure 6 shows the radial distribution dL_{esc}/dr for mini-discs with three different l_0 around a black hole with spin parameter $a_* = 0.9$. Most of the luminosity is produced in the region $r_g < r < 1.4r_g$ where the infall velocity relative to the disc is large and hence a large energy is released in the disc-infall interaction.

We define the radiative efficiency of the disc as the ratio of the total luminosity radiated to infinity, $L_{\text{esc}} = L_{\text{esc}}(r_h)$, to the rest-mass flux through the disc,

$$\eta_{\text{esc}} = \frac{L_{\text{esc}}}{\dot{M}(r_h)c^2}. \quad (35)$$

If the light capture into the black hole is ignored, i.e. L_{esc} is replaced by L , the efficiency is given by

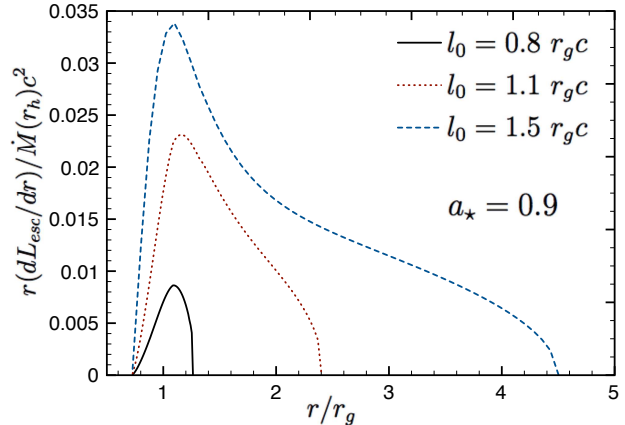


Figure 6. Radial distribution of escaping luminosity for discs with $l_0/r_g c = 0.8, 1.1$, and 1.5 around a black hole with spin parameter $a_* = 0.9$. The luminosity is normalized by the rate of rest-mass accretion through the disc, $\dot{M}(r_h)c^2$.

$$\eta = \frac{L(r_h)}{\dot{M}(r_h)c^2} = 1 + \frac{u_t(r_h)}{c}. \quad (36)$$

We evaluated numerically the dependence of η on the two parameters of the mini-disc l_0 and a_* (Fig. 7). This dependence may be better understood if we express $u_t(r_h)$ in terms of $u^r(r_h)$ and $u_\phi(r_h)$ from $u_i u^i = -c^2$; then equation (36) yields

$$\eta = 1 - \left(1 + \sqrt{1 - a_*^2} \right)^{1/2} \frac{|u^r(r_h)|}{c\sqrt{2}} - a_* \left(1 + \sqrt{1 - a_*^2} \right)^{-1/2} \frac{u_\phi(r_h)}{r_g c}. \quad (37)$$

If $a_* = 0$ this equation simplifies to $\eta = 1 - |u^r(r_h)|/c$ and gives a monotonic dependence of η on l_0 : flows with larger angular momenta have smaller $|u^r(r_h)|$ (their radial motion is centrifugally decelerated) and higher η . In the case of a rotating black hole, equation (37) has additional terms which lead to a complicated dependence of η on l_0 and a_* . For instance, when $a_* = 0.9$ the dependence of η on l_0 is not monotonic (Fig. 7).

The efficiency η is generally increasing with increasing spin of the black hole. It is especially high for retrograde discs, which are described by the solutions with $a_* < 0$. In this case, the second term on the right-hand side of equation (37) is positive and can substantially increase η . A remarkable feature of retrograde discs is that they can extract energy from the black hole via a hydrodynamic analog of Penrose process. This occurs if a_* is close to -1 ; in such discs $u_t(r_h) < 0$ and $\eta > 1$. The maximum $\eta = 1.1$ is reached when $a_* = -1$ and $l_0 = l_{cr}(-1) = 3.15r_g c$.

Next, we evaluated numerically the efficiency η_{esc} that takes into account the capture of the produced radiation into the black hole (Fig. 8). This effect greatly reduces the observed luminosity. The reduction is especially significant for retrograde discs because their radiation is Doppler-beamed in the direction opposite to the black hole rotation, so most of their radiation misses the escape cones shown in Figure A1. The resulting efficiency η_{esc} is highest for prograde discs around maximally rotating black holes ($a_* = 1$). The maximum η_{esc} is close to 10 per cent.

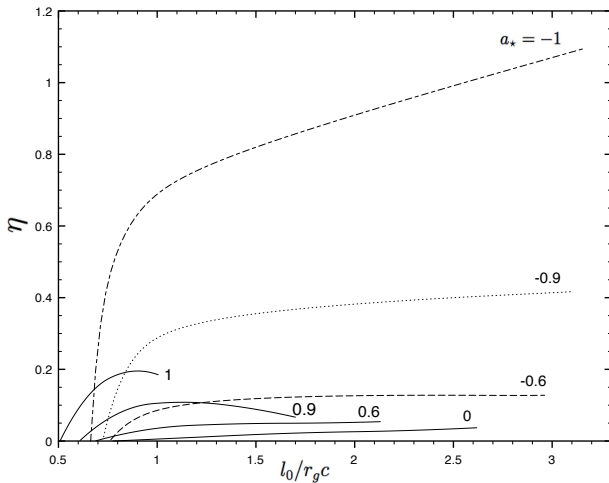


Figure 7. Radiative efficiency as a function of l_0 , ignoring the light capture into the black hole. Seven curves are plotted for black holes with different spin parameters a_* . Solid curves are used for $a_* \geq 0$ and broken curves for $a_* < 0$.

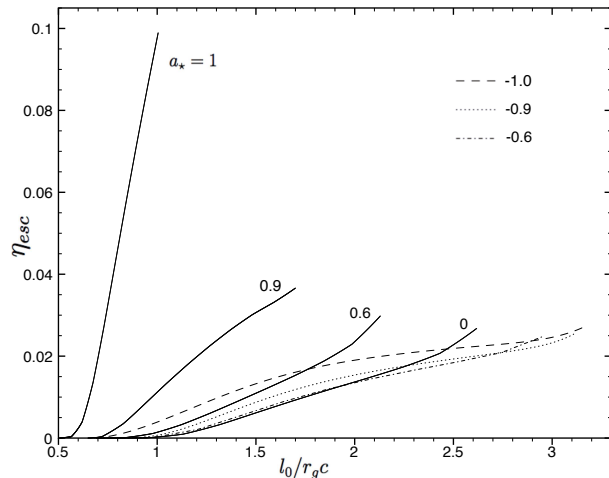


Figure 8. Same as Fig. 7 but taking into account the suppression of radiative efficiency due to light capture into the black hole.

5 CONCLUSIONS

In our model, the mini-disc is completely described by two parameters: the maximum angular momentum of the accreting gas l_0 and the spin parameter of the black hole a_* . $l_0 = 0$ corresponds to spherical accretion. The inviscid mini-disc forms when l_0 is in the range $l_*(a_*) < l_0 < l_{cr}(a_*)$ shown in Fig. 4.

When the black hole rotates in the same direction as the accretion flow ($a_* > 0$), this range becomes smaller compared to the Schwarzschild case and the maximum possible size of the mini-disc is reduced. For example, for the typical $a_* \sim 0.9$ expected in collapsars we find $l_{cr} \approx 1.5r_g c$, which corresponds to a disc of radius $r_d \approx 6r_g = 12GM/c^2$. The mini-disc model may describe collapsars at the early stage when the disc grows from the black hole horizon r_h

to $\sim 12GM/c^2$; then it must switch to the standard viscous regime.

We have calculated the radiative efficiency of mini-discs taking into account the effect of photon (or neutrino) capture into the black hole (Fig. 8). The efficiency is maximum when the mini-disc has its maximum size, near the transition to the viscous-disc regime. For prograde discs around rapidly rotating black holes, the efficiency approaches 0.1, which is ~ 3 times higher than for non-rotating black holes.

We have also studied the case of retrograde discs, where the disc and the black hole are counter-rotating ($a_* < 0$). Such discs can form in wind-fed X-ray binaries where gas accretes with alternating angular momentum due to fluctuations and ‘flip-flop’ instability (e.g. Shapiro & Lightman 1976; Blondin & Pope 2009 and refs. therein). We find that a hydrodynamic analog of Penrose process works in such discs if a_* is close to -1 , i.e. the black hole is close to maximum rotation. Then the black hole accretes matter with negative orbital energy, which means that energy is extracted from the black hole. However, if the extracted energy is radiated quasi-isotropically in the disc rest-frame, most of the produced radiation ends up inside the black hole, and the escaping luminosity is suppressed.

REFERENCES

- Beloborodov A. M., 2008, AIP Conference Proceedings, 1054, 51
 Beloborodov A. M., Illarionov A. F., 2001, MNRAS, 323, 167
 Blondin J. M, Pope T. C., 2009, arXiv:0905.2769
 Bondi H., 1952, MNRAS, 112, 195
 Chandrasekhar S., 1998, The Mathematical Theory Of Black Holes. Oxford University Press, Oxford.
 Illarionov A. F., Beloborodov A. M., 2001, MNRAS, 323, 159
 Illarionov A. F., Sunyaev R. A., 1975, A&A, 39, 185
 Landau L. D., Lifshitz E. M., 1980, The Classical Theory of Fields. Butterworth-Heinemann
 Lee W. H., Ramirez-Ruiz E., 2006, ApJ, 641, 961
 Misner C. W., Thorne K. S., Wheeler J. A., 1973, Gravitation. Freeman, San Francisco
 Rybicki G. B., Lightman A. P., 1979, Radiative Processes in Astrophysics. Wiley, New York
 Shakura N. I., Sunyaev R. A., 1973, A&A, 24, 337
 Shapiro S. L., Lightman A. P., 1976, ApJ, 204, 555

APPENDIX A: CALCULATION OF THE ESCAPING LUMINOSITY

A1 Angular distribution of emission in the local ZAMO frame

Consider an infinitesimal element of the disc, a ring of radius r and thickness δr . It produces luminosity

$$\delta L = \frac{dL}{dr} \delta r = \frac{d}{dr} [(c^2 + cu_t)\dot{M}] \delta r. \quad (\text{A1})$$

The ring emits photons in all directions, which will be parameterized by unit 3D vector $\bar{\Omega}$ in the local frame of ZAMO

(zero-angular-momentum observer at fixed r , see e.g. Misner et al. 1973). Then δL may be written as

$$\delta L = \int_{4\pi} \frac{d(\delta L)}{d\bar{\Omega}} d\bar{\Omega} = \int \frac{d\bar{t}}{dt} \frac{E}{\bar{E}} \frac{d(\delta \bar{L})}{d\bar{\Omega}} d\bar{\Omega}. \quad (\text{A2})$$

Here $\delta \bar{L}$ is the luminosity of the ring measured by ZAMO and \bar{t} is the proper time of ZAMO. E/\bar{E} is the ratio of photon energy measured at infinity, $E = -cv_t$, and measured by ZAMO, $\bar{E} = -c\bar{v}_t = c\bar{v}^t$; this ratio depends on the emission direction $\bar{\Omega}$. It is found from the Lorentz transformation of the photon 4-velocity from the coordinate basis to the (orthonormal) ZAMO basis,

$$\begin{pmatrix} \bar{v}^t \\ \bar{v}^\phi \end{pmatrix} = \begin{pmatrix} \sqrt{-\tilde{g}_{tt}} & 0 \\ g_{t\phi}/\sqrt{g_{\phi\phi}} & \sqrt{g_{\phi\phi}} \end{pmatrix} \begin{pmatrix} v^t \\ v^\phi \end{pmatrix}, \quad (\text{A3})$$

$$\bar{v}^r = \sqrt{g_{rr}}v^r, \quad \bar{v}^\theta = \sqrt{g_{\theta\theta}}v^\theta, \quad (\text{A4})$$

where $\tilde{g}_{tt} = g_{tt} - g_{t\phi}^2/g_{\phi\phi}$. Then one finds,

$$\frac{E}{\bar{E}} = \frac{v_t}{\bar{v}_t} = \sqrt{-\tilde{g}_{tt}} - \frac{g_{t\phi}}{\sqrt{g_{\phi\phi}}}\bar{\Omega}^\phi. \quad (\text{A5})$$

The ratio $d\bar{t}/dt$ appearing in equation (A2) equals $(-\tilde{g}_{tt})^{1/2}$.

The angular distribution of luminosity measured by ZAMO, $d(\delta \bar{L})/d\bar{\Omega}$, is related to the angular distribution of luminosity in the rest frame of the accreting gas of the disc, $d(\delta L_c)/d\Omega_c$, by the Doppler transformation (see e.g. Rybicki & Lightman 1979),

$$\frac{d(\delta \bar{L})}{d\bar{\Omega}} = \frac{1}{\gamma^4(1 - \beta \cdot \bar{\Omega})^3} \frac{d(\delta L_c)}{d\Omega_c}, \quad (\text{A6})$$

where β is the disc velocity (in units of c) measured by ZAMO. We assume that emission is approximately isotropic in the gas frame, i.e. $d(\delta L_c)/d\Omega_c = \delta L_c/4\pi$. Substitution of equations (A5) and (A6) to equation (A2) gives,

$$\delta L = \frac{\delta L_c}{4\pi} (-\tilde{g}_{tt})^{1/2} \int_{4\pi} \frac{[\sqrt{-\tilde{g}_{tt}} - (g_{t\phi}/\sqrt{g_{\phi\phi}})\bar{\Omega}^\phi]}{\gamma^4(1 - \beta \cdot \bar{\Omega})^3} d\bar{\Omega}. \quad (\text{A7})$$

The expression for escaping luminosity δL_{esc} is similar except that the integral is taken over the escape cone S_{esc} rather than 4π . Therefore, the escaping fraction is given by

$$f_{\text{esc}} \equiv \frac{\delta L_{\text{esc}}}{\delta L} = \left(\int_{4\pi} \frac{[\sqrt{-\tilde{g}_{tt}} - (g_{t\phi}/\sqrt{g_{\phi\phi}})\bar{\Omega}^\phi]}{\gamma^4(1 - \beta \cdot \bar{\Omega})^3} d\bar{\Omega} \right)^{-1} \times \int_{S_{\text{esc}}} \frac{[\sqrt{-\tilde{g}_{tt}} - (g_{t\phi}/\sqrt{g_{\phi\phi}})\bar{\Omega}^\phi]}{\gamma^4(1 - \beta \cdot \bar{\Omega})^3} d\bar{\Omega}.$$

Evaluating the integral over 4π we obtain equation (34).

A2 Escape cones

The photon direction in the ZAMO frame, $\bar{\Omega}$, can be described by two angles α and φ ,

$$\bar{\Omega}^r = \frac{\bar{v}^r}{\bar{v}^t} = \cos \alpha, \quad (\text{A8})$$

$$\bar{\Omega}^\theta = \frac{\bar{v}^\theta}{\bar{v}^t} = \sin \alpha \sin \varphi, \quad (\text{A9})$$

$$\bar{\Omega}^\phi = \frac{\bar{v}^\phi}{\bar{v}^t} = \sin \alpha \cos \varphi. \quad (\text{A10})$$

Using the relations between \bar{v}^i and v^i (eqs. A3 and A4), we express $\bar{\Omega}$ in terms of v^i ,

$$\cos \alpha = \sqrt{-\frac{g_{rr}}{\tilde{g}_{tt}}} \frac{v^r}{v^t} = \frac{\sqrt{r^4 + a^2 r(r+r_g)} v^r}{a^2 + r(r-r_g) v^t}, \quad (\text{A11})$$

$$\sin \alpha \sin \varphi = \sqrt{-\frac{g_{\theta\theta}}{\tilde{g}_{tt}}} \frac{v^\theta}{v^t} = \sqrt{\frac{r^4 + a^2 r(r+r_g)}{a^2 + r(r-r_g)}} \frac{v^\theta}{v^t}, \quad (\text{A12})$$

where all metric coefficients have been evaluated at the equatorial plane at the emission radius r .

The photon 4-velocity v^i is expressible in terms of four integrals of motion in Kerr metric: energy E , total angular momentum L , its projection L_z , and Carter integral Γ . Using these expressions (see e.g. Chandrasekar 1982) and choosing the affine parameter along the photon worldline so that $E = c^2$, we find v^r/v^t and v^θ/v^t as functions of r , Γ and L_z , and obtain

$$\begin{aligned} \cos^2 \alpha &= \frac{r^4 + a^2 r(r+r_g)}{[r^4 + a^2 r(r+r_g) - r_g a L_z r]^2} \\ &\times [r^4 + r^2(\Gamma + a^2) + r r_g (a^2 - \Gamma - 2a L_z) \\ &+ a^2(\Gamma + L_z^2)], \end{aligned} \quad (\text{A13})$$

$$\begin{aligned} \sin^2 \alpha \sin^2 \varphi &= -(\Gamma + L_z^2)(r^2 + a^2 - r_g r) \\ &\times \frac{[r^4 + a^2 r(r+r_g)]}{[r^4 + a^2 r(r+r_g) - r_g a L_z r]^2}. \end{aligned} \quad (\text{A14})$$

Equations (A13) and (A14) can be solved for L_z and Γ for given r , α and φ .

The fate of a photon is determined by the equation of radial motion for null geodesics (e.g. Chandrasekar 1982),

$$\begin{aligned} (r^2 + a^2 \cos^2 \theta)^2 (v^r)^2 &= (r^2 + a^2 - r_g r)(\Gamma - a^2 E^2) \\ &+ (r^2 + a^2)^2 E^2 - 2r_g a E L_z r + a^2 L_z^2, \end{aligned} \quad (\text{A15})$$

where $E = c^2$ with our choice of affine parameter along photon worldline. The possible turning points r_{turn} are found from the condition $v^r = 0$. Let r_0 be the initial radial position of the photon. Two cases are possible: (i) $v(r_0) > 0$, the photon escapes if there are no $r_{\text{turn}} > r_0$. (ii) $v(r_0) < 0$, the photon escapes if there is at least one turning point such that $r_h < r_{\text{turn}} < r_0$ and no $r_{\text{turn}} > r_0$.

For any given direction $\bar{\Omega}$, we find L_z and Γ from equations (A13) and (A14), then determine the roots r_{turn} of equation $v^r(r) = 0$ and check the escape conditions. All escaping directions form the ‘‘cone’’ S_{esc} on the sky of ZAMO, which is found numerically. Figure A1 shows the escape cones for five emission radii r_0 and four values of a_* .

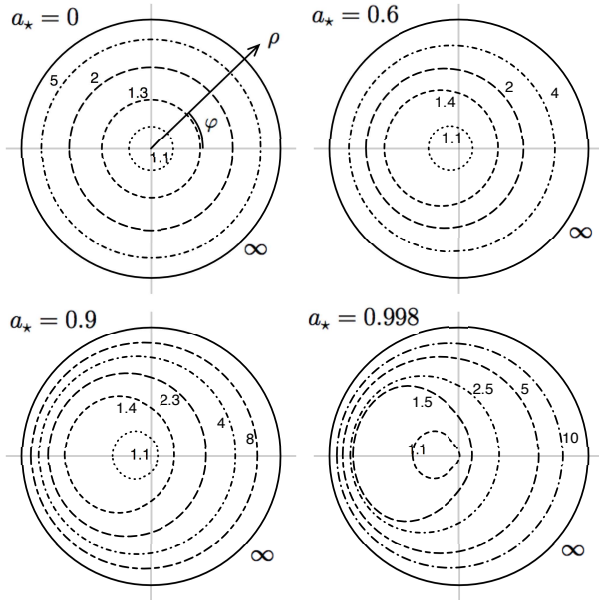


Figure A1. Escape cones S_{esc} on the ZAMO sky. The photon direction $\bar{\Omega}$ is specified by two angles α and φ (eqs. A8-A10). The figure uses polar coordinates (ρ, ϕ) with $\rho = \alpha/\pi$ to represent all possible photon directions. The origin of the diagram $\rho = 0$ corresponds to the radial direction away from the black hole (such photons always escape) and the unit circle $\rho = 1$ (thick black curve) corresponds to the radial direction into the black hole (such photons are captured). The colour curves show the boundary of the escape cone for five emission radii; the emission radius is indicated next to the curves, in units of the horizon radius r_h . The figure presents four such diagrams calculated for black holes with spin parameter $a_* = 0, 0.6, 0.9,$ and 0.998 .